Stress/Strain Development Around a Spherical Inclusion in a Polymeric Matrix: The Effects of Particle and Matrix Mechanical Characteristics and Thermal Expansivity Difference

Dariush Hosseinpour,[1] John C. Berg[2]

[1]*Chemical Engineering Department, Lehigh University, Bethlehem, Pennsylvania 18015*
[2]*Chemical Engineering Department, University of Washington, Seattle, Washington 98195*

Received 29 October 2011; accepted 18 January 2012
DOI 10.1002/app.36855
Published online in Wiley Online Library (wileyonlinelibrary.com).

ABSTRACT: For a spherical inclusion embedded in an infinite polymeric matrix, the Goodier Model, combined with thermal stress contribution, is applied to establish the stress/strain fields around a spherical particle in different particle/matrix combinations, including TiO_2, alumina, silica, steel, polystyrene, and polyvinyl butyral particles embedded in a range of polymeric matrices. This approach provides the basis for examining the effects of different parameters such as Young's modulus and Poisson's ratio of the particle and matrix, and the thermal history of samples on the failure-initiation criteria. An explanation is provided for divergent results obtained for very soft and elastic particles. © 2012 Wiley Periodicals, Inc. J Appl Polym Sci 000: 000–000, 2012

Key words: stress development; strain development; particle-filled composite; Goodier Model; Young's modulus; Poisson's ratio; Coating composites; thermal expansion coefficient

INTRODUCTION

Filled polymers are among the simpler types of composite material, consisting of a matrix polymer, as the continuous phase, and a discrete phase, generally inorganic particulate and/or organic particulate, (with or without organic/inorganic surface treatment), dispersed in the matrix. Particulates, including pigments and fillers are used to modify the various properties of polymers (mechanical properties, corrosion protection, conductivity, color appearance, and etc.) that are of great importance to coating composites.[1,2]

Whatever the intended purpose of the introduction of the filler, when particles are added to the dispersed phase, the mechanical properties of the resulting composite change. It is essential to have an understanding of the dependence of such properties on the composition in order to be able, effectively and efficiently, to manipulate the system and, ultimately, to obtain an optimal performance of the composite. It is known that during the deformation process of an unfilled polymer, stress builds up at weak points in the matrix structure, resulting in rupture or fracture of the polymer. This local rupture then propagates through the bulk of the specimen. In a filled polymer, failure may be initiated at the polymer/filler interface, within the polymer matrix, as mentioned above, or within the particle agglomerates.[3] Focusing on failure at the polymer/filler interface, the approach and analysis of Goodier[4] has often been used for the calculation of stress distribution around inclusions in the matrix. Goodier's model assumes:

1. A single particle is embedded in a homogeneous, infinite matrix
2. There is perfect adhesion between the phases
3. There is an equilibrium of stresses and displacements at the interface
4. There is a homogeneous external load.

In fact, the description of stresses that exist at the interface of a spherical inclusion, submitted to a uniaxial tensile field, is a two-part problem requiring determination of;

1. The stresses at the interface because of the applied stress field, using the Goodier's model.
2. The thermal stresses at the interface due to differences in the coefficient of thermal expansivity.

Goodier's derivation ignores the possible presence of any stress that might exist around the spherical inclusion prior to tensile straining. In reality, the production of any composite featuring dissimilar

Correspondence to: D. Hosseinpour (dah409@lehigh.edu) or J. C. Berg (berg@cheme.washington.edu).

elastic phases, results in thermal stresses at all existing interfaces. These residual stresses, caused by differences in the thermal coefficient of expansivity of the inclusions and the matrix, can develop in the samples simply by heating them to the processing temperature (e.g., curing temperature), and by cooling them down from such a temperature.[5–7] Besides, throughout its lifetime, a coating composite system is subjected to numerous thermal cycles.

Interfacial yielding in a filled composite occurs when a critical limit, or "failure criterion" is reached. The following represent the most common yield criteria as applied to an isotropic material (uniform properties in all directions):

1. Maximum principal strain. Yield occurs when the maximum principal strain reaches the strain corresponding to the yield point during a simple tensile test.
2. Maximum principal stress. Yield occurs when the largest principal stress exceeds the uniaxial tensile yield strength.
3. Maximum dilation. On the basis of this criterion, yielding occurs when the change in volume per unit volume, referred to as dilation, reaches a critical value.
4. Maximum strain energy. This criterion assumes that the stored energy associated with elastic deformation at the point of yield is independent of the specific stress tensor. Thus yield occurs when the strain energy per unit volume is greater than the strain energy at the elastic limit in simple tension.
5. Maximum distortion energy or maximum principal shear. This criterion is based on the determination of the distortion energy in a given material, i.e., of the energy associated with changes in the shape in that material. According to this criterion, a given structural material is safe as long as the maximum value of the distortion energy per unit volume in that material remains smaller than critical distortion energy per unit volume.

To establish the locations of failure-initiation according to the five criteria described above, one needs to compute the distributions of principal strain, the principal stress, dilatational strain, strain energy, and distortion energy in the polymeric matrix that surrounds the inclusion. The thermal stress contribution to these criteria, are obtained through combining the Goodier's solution with equations derived by Beck et al.[8] and Wang et al.,[9] as summarized in Appendix.

Although the model has been in existence for some time, there has not been, to the best of our knowledge, a parametric study addressing stress distribution at the interface for a range of particle/matrix combinations commonly used in coating composite industry. In this work, the objective is to provide a description of how changes in particle or polymeric matrix properties changes the stress/strain field at the interface and hence influences failure development in a composite. Such reformulations are common practice in the coating industry for a variety of reasons, including changing the coating color through changing the pigment and coating reinforcement via particle introduction. It is also common to make changes in processing or coating temperature. Descriptions of the effects of such changes are important if one is to understand how failure develops in a coating composite system. Such understanding can positively contribute to design, formulation as well as reformulation, processing and performance of coating composites.

Modeling the stress distribution around inclusions in the polymeric matrix

The approach here concerns a single spherical inclusion embedded in an infinite polymeric matrix, as treated by the Goodier model[4] combined with the contribution from thermal stresses, to establish the failure criteria for such a system. Table I provides the list of materials investigated and their physical properties. To ascertain the failure criteria, equations described in Appendix were solved as visual basic macros in Excel.

Figure 1 shows the distribution of the criteria for the interface of a TiO_2 spherical particle in a poly (methyl methacrylate) (PMMA) matrix under a simple tension of $T = 20$ MPa. The curves are plotted over $\theta = 0^\circ$ to $\theta = 90^\circ$ as they are symmetric with respect to the equatorial plane ($\theta = 90^\circ$) and the polar axis ($\theta = 0^\circ$) of the TiO_2 particulate.

Considering that the failure will initiate at the interface/interphase between the matrix and the particulate (with values larger than unity), the five craze-initiation manifestations (Fig. 1) suggest that the failure would initiate at different locations (i.e., different maximal angles for different failure-initiation manifestations).

Among these manifestations, the principal strain and the strain energy characteristic properties have been reported to agree best with the test data.[9] In particular, the concept of the principal strain criterion seems to be plausible from the suggestion that crazing is usually preceded by a certain degree of local reorientation in molecular structures.[10] Since the molecular orientation is more directly related to strain than that to stress or strain energy, if one regards failure as a highly localized straining process, then invoking the principal strain criterion would seem to be more reasonable for describing

TABLE I
Physical Properties of Materials Used to Calculate the Craze-Initiation Criteria for a Single Spherical Particulate That Is Embedded in an Infinite Polymeric Matrix

	Material Function	Young's Modulus MPa	Poisson's Ratio	Thermal Expansion Coefficient $(°C)^{-1}$
TiO_2	Filler	2.82E+05	0.28	7.00E-6
Alumina (alpha)	Filler	3.70E+05	0.22	7.00E-07
Steel	Filler	2.10E+05	0.28	1.08E-05
silica	Filler	7.00E+04	0.17	9.00E-06
Polystyrene	Filler/Matrix	3.20E+03	0.35	1.20E-04
PVB	Filler/Matrix	9.50E+02	0.5	4.68E-04
Epoxy	Matrix	2.40E+03	0.35	5.50E-05
PMMA	Matrix	1.80E+03	0.35	7.50E-06
Polycarbonate	Matrix	2.35E+03	0.37	6.80E-05
Polyimide	Matrix	2.50E+03	0.34	4.50E-05
PP	Matrix	1.20E+03	0.45	1.40E-04
PVC Hard	Matrix	3.25E+03	0.38	8.75E-05
Nylon 6,6	Matrix	3.30E+03	0.41	9.00E-05

the craze-initiation behavior than would consideration of other criteria.[9] Therefore, in the following discussion, the principal strain will be regarded as the main indicating criterion in obtaining failure-initiation location on the particle surface.

The effect of particle characteristics

To establish whether or not the particle characteristics such as its rigidity would influence the maximum of the principal strain as a failure-initiation criterion, the values of principal strain were calculated over $\theta = 0°$ to $\theta = 90°$ for particles having different rigidity values, moduli, and thermal expansion coefficients.

Figure 2 provides principal strain distributions along the interface for different particles namely, TiO_2, alumina (alpha), silica, steel, Polyvinyl butyral, and Polystyrene each embedded in a PMMA polymeric matrix at a tensile stress of $T = 20$ MPa, over $\theta = 0°$ to $\theta = 90°$. As evidenced by the results, the nature of particle plays an important role on how the strain (as well as stress) is distributed around the particle. Based on the principal strain distribution, three different categories can be identified:

1. Particles that are considerably softer than the matrix (e.g., PVB particle embedded in a PMMA matrix). The distribution of maxima for

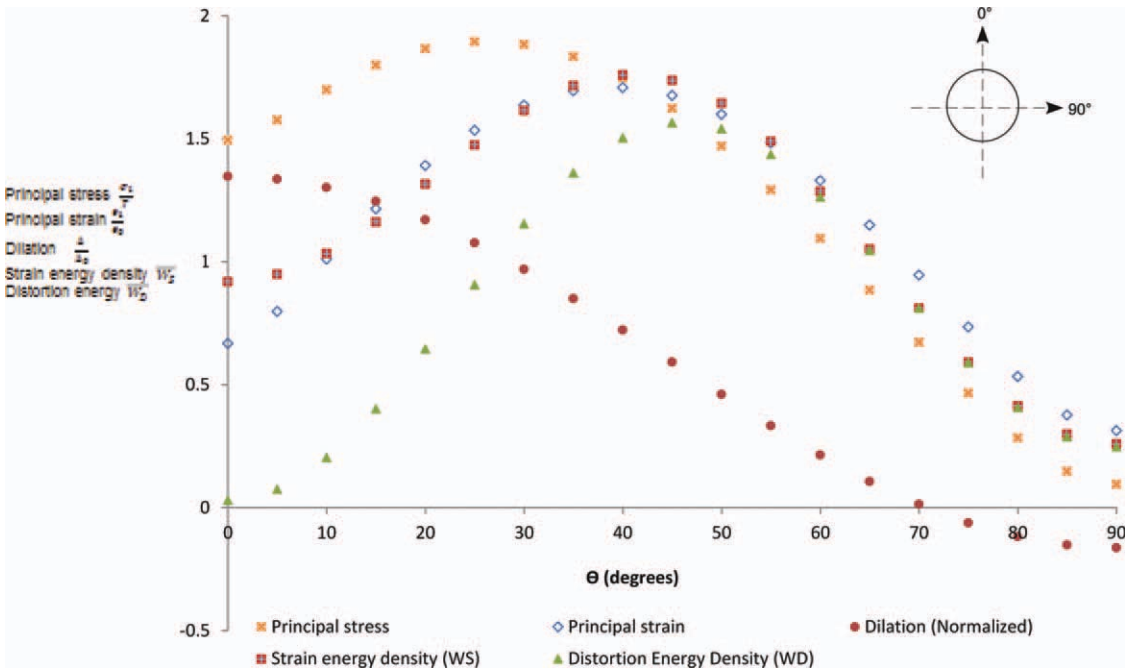

Figure 1 The distribution of the failure initiation criteria around a single spherical TiO_2 particle embedded in a PMMA matrix at tensile stress of $T = 20$ MPa and the temperature difference of $-60°C$ over $\theta = 0°$ to $\theta = 90°$. [Color figure can be viewed in the online issue, which is available at wileyonlinelibrary.com.]

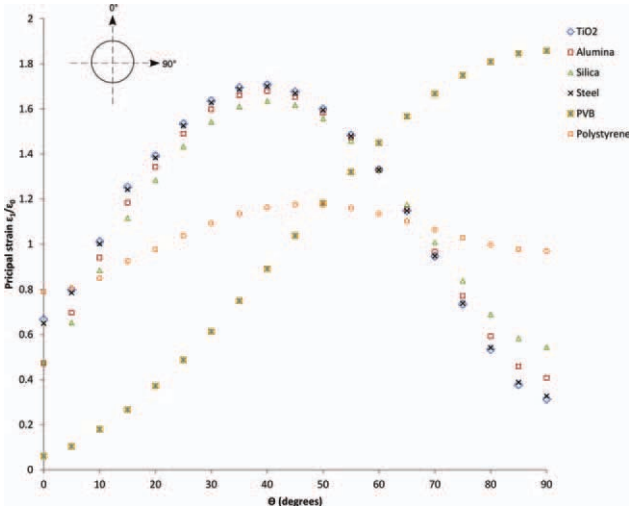

Figure 2 The distribution of the normalized principal strain around different particles each embedded in a PMMA polymeric matrix over $\theta = 0^\circ$ to $\theta = 90^\circ$. The modeling was conducted for a tensile stress of $T = 20$ MPa and a temperature difference of $\Delta t = -60$°C. [Color figure can be viewed in the online issue, which is available at wileyonlinelibrary.com.]

this case is located close to the equator, and therefore, one would expect, statistically, the location for failure under tensile stress to be around the equator.

2. Particles that are considerably harder than the matrix (e.g., TiO_2, alumina, silica, steel in PMMA matrix). For this case, the maxima have shifted about 50° towards the pole position.
3. Particle properties (mechanical and thermal) are not significantly different from those of matrix (e.g., a PS particle in a PMMA matrix). The principal strain distribution for this case does not change considerably over $\theta = 0^\circ$ to $\theta = 90^\circ$ as noticed for the two previous categories.

Such observations can be generalized by recognizing that for particles that are far more rigid than the continuous matrix, the failure will initiate at a location that is farther than the equator position. For particles that are softer than the matrix, failure initiation will occur around the equator of particle in the matrix.[11]

The effect of polymeric matrix characteristics

Given the diversity of different polymeric chemistries used as the matrix in filled polymeric composites, we were also interested in the stress and strain development around a single spherical particle embedded in different polymeric matrices. Figure 3 provides the distribution of normalized principal strain at a TiO_2 spherical particle interface embedded in different polymeric matrices. It is evident that the nature of polymeric matrix plays an important role in the strain (as well as stress) level that builds at the interface as well as its distribution. The peak max for the TiO_2/PS system is about 50% greater than the one for TiO_2/PVB system. Assuming the same adhesion strength for both interfaces, the TiO_2/PS interface would be more prone to failure when compared to the interface at TiO_2/PVB or TiO_2/Polypropylene system. From the trend seen in Figure 3, one can conclude that a greater value for matrix Young's modulus and a smaller value for matrix Poisson's ratio contribute to a larger strain development at the rigid filler/polymer interface. Another observation from Figure 3 is that by changing the polymeric matrix from PVB to PS, the location of the maximum strain at the interface shifts by about 10° towards the pole position.

The effect of thermal conditions

Since the thermal-expansion coefficients of the inclusions and the matrix are different, thermal stresses can develop in the samples simply on cooling the samples from the processing temperature (e.g., annealing or curing). For heat-cured coatings, heating the inclusion-matrix sample up to the curing temperature followed by cooling it down to the room temperature, would also induce thermal stresses into the system, due to the mismatch in the thermal-expansion coefficients. To understand how the thermal conditions may influence the strain development around a particle embedded in a polymeric matrix (i.e., TiO_2 in PMMA), its distribution at the interface was calculated under different thermal conditions. The results for the effect of thermal conditions are presented in Figure 4.

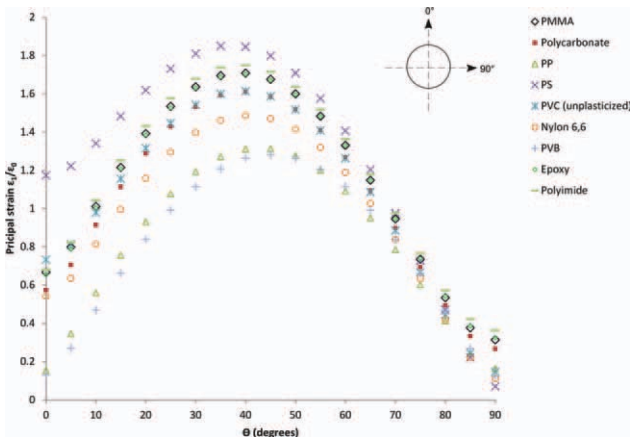

Figure 3 Distribution of normalized principal strain around a TiO_2 particle embedded in different polymeric matrices. The modeling was conducted over $\theta = 0^\circ$ to $\theta = 90^\circ$ for a tensile stress of $T = 20$ MPa. The temperature difference was −60°C. [Color figure can be viewed in the online issue, which is available at wileyonlinelibrary.com.]

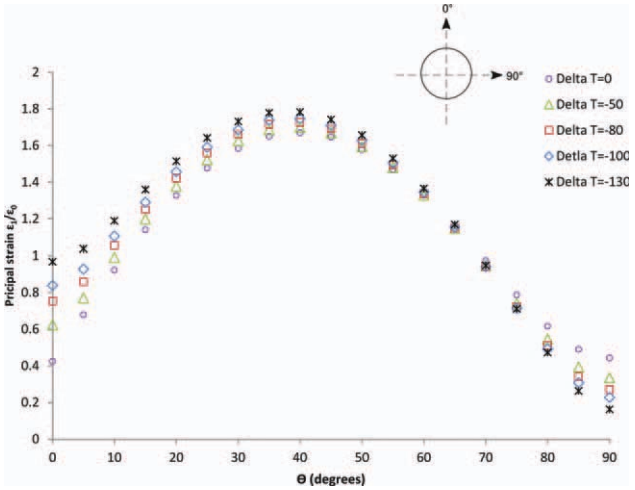

Figure 4 The effect of thermally induced stress on the distribution of the normalized principal strain around the TiO_2 particle that is embedded in a PMMA matrix. The modeling was conducted over $\theta = 0^\circ$ to $\theta = 90^\circ$ for a tensile stress of $T = 20$ MPa. [Color figure can be viewed in the online issue, which is available at wileyonlinelibrary.com.]

As the system experiences a higher temperature (Fig. 4), more strain (as well as stress) around the inclusion develops, as evidenced by the area under the distribution curve. The maximum principal strain for TiO_2/PMMA increases by 8% once subjected to a process with a $\Delta T = -100$°C cooling step, as opposed to an isothermal one. Another observation is that, through subjecting the system to a process with a thermal history, the distribution becomes more unsymmetrical over $\theta = 0^\circ$ to $\theta = 90^\circ$, with more strain developments at lower angles (angles smaller than 65°) and a decrease in the strain level at locations closer to the equator.

The effect of varying the external tension on the stress/strain distribution at the particle/matrix interface is shown in Figure 5, which depicts the distribution of the normalized principal stress around a spherical TiO_2 particle embedded in a PMMA matrix. At higher loads, the normalized principal stress decreases at locations closer to the pole, and also the shape of principal stress over $\theta = 0^\circ$ to $\theta = 90^\circ$, becomes more symmetric with respect to the 45° polar angle. It should be noted that the figure depicts normalized stress values, which may be misleading, in that while the absolute maximum value of the principal stress increases, the normalized value decreases. The principal stress distribution without normalization has been plotted in Figure 6 as a function of different external loads. The information in Figure 6 would be important from a composite design standpoint, as a practical guideline for the minimum required adhesion strength level between particle and interface. For example for the TiO_2/PMMA composite system under a simple tensile stress of 100MPa, the adhesion strength between TiO_2 particle and PMMA has to be above 186 MPa to avoid debonding at the interface.

Considering that the particle/matrix adhesion is uniform for all angles at the interface, failure would start at the interface when the stress there exceeds a critical value defined by the yield stress (or a strain) exceeds critical strain value. Once failure is initiated at the interface, the propagation path could be through one or a combination of the following:

1. The bulk of the matrix
2. The bulk of particle
3. The particle/matrix interface

As a practical matter, the analysis is limited to cases of moderate adhesion. When the adhesion is very strong, the sample fails cohesively through the

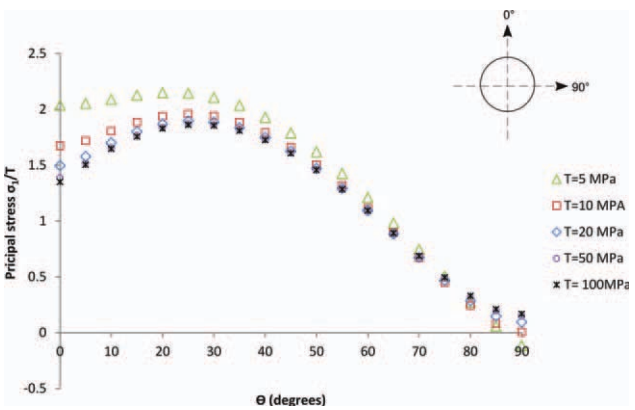

Figure 5 The distribution of the normalized principal stress over $\theta = 0^\circ$ to $\theta = 90^\circ$ around a TiO_2 particle embedded in PMMA for different simple tension loads. The modeling was conducted for a temperature difference of −60°C. [Color figure can be viewed in the online issue, which is available at wileyonlinelibrary.com.]

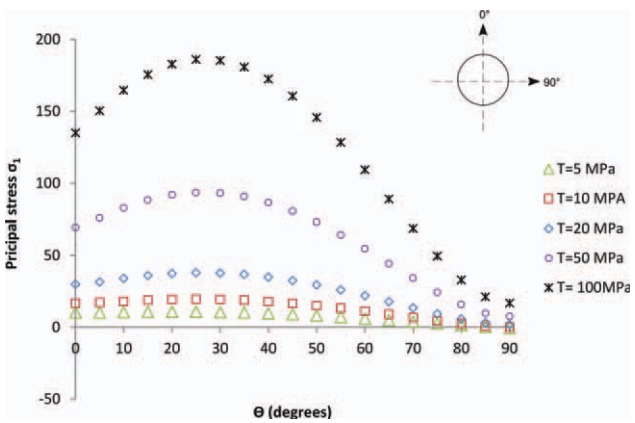

Figure 6 The distribution of the principal stress over $\theta = 0^\circ$ to $\theta = 90^\circ$ around a TiO_2 particle embedded in PMMA for different external tensile loads. The modeling was conducted for a temperature difference of −60°C. [Color figure can be viewed in the online issue, which is available at wileyonlinelibrary.com.]

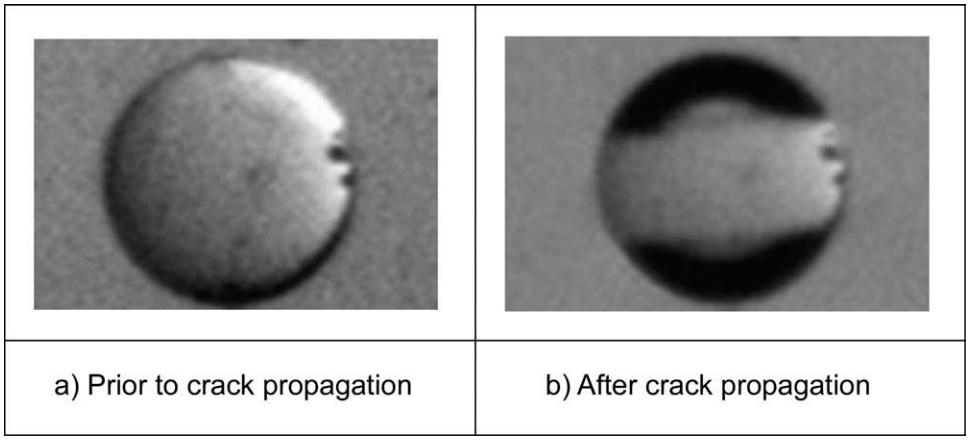

Figure 7 Glass spherical particle in a PVB matrix under the external stress (a) prior to crack propagation and (b) after crack propagation.

formation of crazes in the region of the maximum principal stress.[11] For typical filled coating composites, the interface is the weakest point, and hence prone to crack propagation. For a rigid particle embedded in a polymeric matrix (e.g., TiO_2/PMMA), once the cavitation develops at a location with maximum stress build-up (i.e., $\theta \sim 30^\circ$), then for crack propagation as the next phase, either one or a combination of the following may happen in a two-dimensional system:

1. The crack would propagate toward the equator at the interface
2. The crack would propagate toward the pole at the interface

On the basis of the stress and strain level distribution calculated, it seems that the crack would propagate first toward the pole position, as this path is experiencing higher stress level (or strain level) compared to the one toward the equator. Besides, under simple external tensile stress (shown in Fig. 1), the perpendicular component for crack opening toward pole is more pronounced than the one toward the equator. Once the crack reaches the pole, a debonded area in the shape of a cap develops around the pole, and the stress would intensify in the remaining intact area at the interface, which still bears the stress. In the next phase, the crack would propagate toward the equator.

In corroboration of the above statement are the results of a test in which a single glass bead of 300 μm diameter was incorporated in a PVB matrix.[5,6] Figure 7 shows the particle before and after failure under stress, with the dark region showing the debonded area. The authors reported that debonding was observed to propagate from the polar region toward the equator after decapping completion in the polar region.

We were also interested in finding out the stress and strain values at the particle/matrix interface for systems in which the particle is much softer than the matrix. Examples for this case include very soft rubber particles incorporated in rigid polymeric matrices and also air bubbles trapped in the polymeric matrix. Under isothermal conditions, there is a significant mismatch between matrix and particle in terms of their Young's moduli and Poisson's ratios.

Assuming that a very soft particle has been incorporated in a PMMA matrix, different Young's modulus and Poisson's ratio values associated with these particles (i.e., $E \rightarrow 0$ and $\nu \rightarrow 0.5$) were used to calculate the principal strain at the particle/matrix interface. Principal values are given in Table II. The results indicate that the principal strain increases significantly when the embedded particle become softer (i.e., $E \rightarrow 0$ and $\nu \rightarrow 0.5$). The divergence is caused as the denominators in Terms A and C (eq. A9 and A10 in Appendix) approach zero. The results may in fact be real, i.e., the principal strain

TABLE II
Principal Values at 0 and 90° for Soft Particles of Different Young's Moduli and Poisson's Ratios Embedded in PMMA Polymeric Matrix Under Isothermal Conditions (Δt = 0°C)

ν_1 (Particle Poisson's ratio)	0.5	0.5	0.5	0.5	0.4999	0.499	0.49	0.49	0.49	0.49
E_1(Particle Young's modulus)	0	0.001	0.1	1	0	0	0	1	10	100
Principal strain at 0°	∞	524209.74	5243.15	525.27	969.83	98.34	11.19	11.00	9.61	4.61
Principal strain at 90°	∞	524208.34	5241.75	523.87	968.43	96.94	9.79	9.60	8.20	3.20

actually should diverge as the particle with a Poisson's ratio approaching 0.5, becomes significantly compliant. However, the divergence in practice, especially for the interfacial stress, may be unrealistic, owing to possible shortcomings of the Goodier Model under these conditions. Understanding the exact cause of the apparent divergence needs further investigation.

In the context of present study, the following remarks regarding the Goodier model should be noted:

1. The particle is assumed to be spherical. In practice, for a particle, there would be a deviation from being a perfect sphere, which would influence the results of the Goodier Model in terms of stress distribution around the particle.[12]
2. The Goodier Model assumes only one particle is incorporated in an infinite matrix. Particle-filled composites represent much more complex systems in which many particles are incorporated in the matrix in such a way that stress field around each individual particle interacts with those of the neighboring particles.[13,14] Such interaction would change the stress distribution outcome around each particle. The matrix size in practice is not infinite, and therefore the boundaries of interface would be influential in the stress distribution within the composite as well as in the composite response to the external stress. The model also does not take into account the role of particle size. This size would be more influential if ratio of particle size to composite size increases.
3. Particle aggregation is clearly beyond the scope of the model. In practice, aggregates are present to some extent in particle-filled composites. Such a presence would result in wetting anomalies caused by either particle/particle touching or air pockets trapped between aggregate particles. In either case, the stress distribution around each particle within the aggregate would deviate from the one produced by the model. Aggregates are known to function as stress concentration centers in filled composite systems, which can result in premature failure.
4. Despite its shortcomings, the Goodier Model provides a platform for the incorporation of additional parameters so that it may better represent real composite systems. This was the basis for revisiting the modified Goodier Model in the present study. The results clearly showed strong dependence of stress/strain fields around particle on mechanical characteristics of both particle and matrix and well as on the thermal history.

The authors thank Dr. Felix Nguyen from Toray Composites for invaluable discussions.

APPENDIX

Goodier chose a spherical coordinate system (r, ϕ, θ) with its origin at the center of inclusion and its polar axis parallel to the applied load, T.[4,8,9]

The fundamental equation for the model is :

$$\nabla\nabla\underline{u} + (1-2\nu)\Delta\underline{u} = 0 \tag{A1}$$

which must be solved under the following boundary conditions:

$$\underline{u}^m(R) = \underline{u}^p(R) \tag{A2}$$

$$(\hat{\sigma})^m(R) = (\hat{\sigma})^p(R) \tag{A3}$$

Here, $\underline{u}$ is the displacement vector, $(\hat{\sigma})$ the stress tensor, ν the Poisson's ratio and R is the radius of the inclusion. The superscripts p and m denote the filler and the matrix respectively (Fig. A1).[15] FA1

By taking into account the thermal stress that may develop in the composites, the nonzero stress components in the matrix, under a simple tension T, may be written as[11]:

$$\frac{\sigma_r}{T} = 4Ax^3 - 20\nu_2 Bx^3 + 24Bx^5 + 2B\left[-10(5-\nu_2)x^3 + 36x^5\right]\times\cos 2\theta + \frac{1}{2}(1+\cos 2\theta) + \frac{4G_2Cx^3}{3T} \tag{A4}$$

$$\frac{\sigma_\theta}{T} = -2Ax^3 - 20\nu_2 Bx^3 - 6Bx^5 + 2B\left[5(1-2\nu_2)x^3 - 21x^5\right]\times\cos 2\theta + \frac{1}{2}(1+\cos 2\theta) - \frac{2G_2Cx^3}{3T} \tag{A5}$$

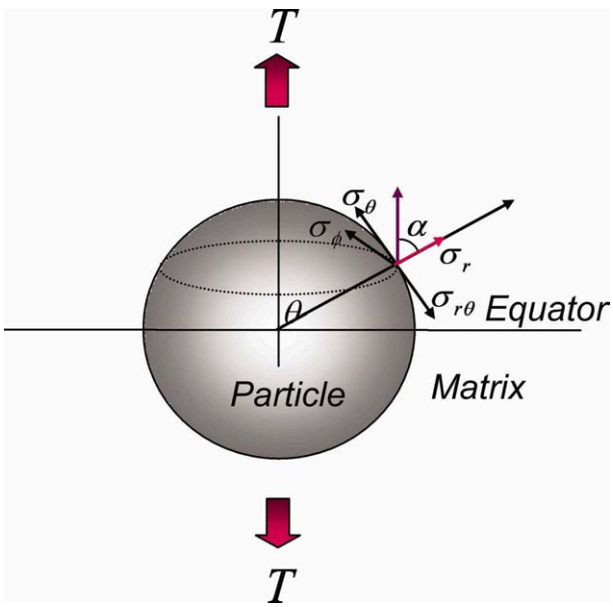

Figure A1 Spherical coordinate system for a spherical particle embedded in a matrix exposed to an external stress, T. [Color figure can be viewed in the online issue, which is available at wileyonlinelibrary.com.]

$$\frac{\sigma_\phi}{T} = -2Ax^3 - 20(1-\nu_2)Bx^3 - 18Bx^5 + 2B\left[15(1-2\nu_2)x^3 - 15x^5\right] \times \cos 2\theta + \frac{2G_2Cx^3}{3T} \quad \text{(A6)}$$

$$\frac{\sigma_{r\theta}}{T} = -\left[20(1+\nu_2)Bx^3 - 48Bx^5 + \frac{1}{2}\right] \sin 2\theta \quad \text{(A7)}$$

Here, r is the distance from the origin to the point, θ is the angle between the positive x-axis and the line from the origin point in the xy-plane and φ is the angle between the z-axis and the line from the origin to the point (Fig. 1). G_2 and ν_2 are the shear modulus and the Poisson's ratio of the matrix material, respectively, and

$$x = a/r$$
$$B = \frac{1}{8}\frac{1-G}{(7-5\nu_2)+(8-10\nu_2)G} \quad \text{(A8)}$$

$$A = B\frac{2(1-2\nu_1)(6-5\nu_2)+(3+19\nu_1-20\nu_1\nu_2)G}{2(1-2\nu_1)+(1+\nu_1)G} + \frac{1}{4}\frac{1(1-\nu_2)(1+\nu_1)/(1+\nu_2)-\nu_1-(1-2\nu_1)G}{2(1-2\nu_1)+(1+\nu_1)G} \quad \text{(A9)}$$

$$C = \frac{(\alpha_1-\alpha_2)(1+\nu_1)G\Delta t}{2(1-2\nu_1)+(1+\nu_1)G} \quad \text{(A10)}$$

Here, "r" is the radius from the center of the inclusion, "a" is the radius of the inclusion, $G = G_1/G_2$. G_1 and ν_1 are, respectively, the shear modulus and the Poisson's ratio of the inclusion, Δt is the temperature difference, and α_1 and α_2 are the linear thermal expansion coefficients of the inclusion and the matrix, respectively. G_2 is the shear modulus of the matrix.

Noting that the stress components other than those listed in eqs. (A4)–(A7) are zero, the principal stresses (σ_1, σ_2, σ_3) at any point in the matrix may be written as;

$$\sigma_{1,2} = \frac{1}{2}(\sigma_r+\sigma_\theta) \pm \frac{1}{2}\left[(\sigma_r-\sigma_\theta)^2+4\sigma_{r\theta}^2\right]^{1/2} \quad \text{(A11)}$$

$$\sigma_3 = \sigma_\phi \quad \text{(A12)}$$

The angle, α, of the direction of the principal stress σ_1, measured from the radial direction is;

$$\alpha = \frac{1}{2}\tan^{-1}\left(\frac{2\sigma_{r\theta}}{\sigma_\theta-\sigma_r}\right) \quad \text{(A13)}$$

The principal shear stresses are:

$$\tau_1 = \frac{1}{2}|\sigma_1-\sigma_2| \quad \text{(A14)}$$

$$\tau_2 = \frac{1}{2}|\sigma_2-\sigma_3| \quad \text{(A15)}$$

$$\tau_3 = \frac{1}{2}|\sigma_3-\sigma_1| \quad \text{(A16)}$$

The maximum principal shear among the principal shear stresses is denoted by τ.

The principal strains (ε_1,ε_2,ε_3) are obtained from eqs. (A11)–(A12) by Hook's law:

$$\varepsilon_1 = \frac{\sigma_1}{E_2} - (\nu_2/E_2)(\sigma_2+\sigma_3) \quad \text{(A17)}$$

$$\varepsilon_2 = \frac{\sigma_2}{E_2} - (\nu_2/E_2)(\sigma_1+\sigma_3) \quad \text{(A18)}$$

$$\varepsilon_3 = \frac{\sigma_3}{E_2} - (\nu_2/E_2)(\sigma_1+\sigma_2) \quad \text{(A19)}$$

Here, E_2 is the Young's modulus of the matrix material. The dilational strain, Δ is then given by;

$$\Delta = \varepsilon_1+\varepsilon_2+\varepsilon_3 = \frac{1-2\nu_2}{E_2}(\sigma_1+\sigma_2+\sigma_3) \quad \text{(A20)}$$

In terms of the principal stresses, the strain energy density, W_S, and the distortion energy density W_D can be expressed as;

$$W_S = -\frac{\nu_2}{2E_2}(\sigma_1+\sigma_2+\sigma_3)^2 + \frac{1+\nu_2}{2E_2}\left(\sigma_1^2+\sigma_2^2+\sigma_3^2\right) \quad \text{(A21)}$$

$$W_D = (12G_2)^{-1}\left[(\sigma_1-\sigma_2)^2+(\sigma_2-\sigma_3)^2+(\sigma_3-\sigma_1)^2\right] \quad \text{(A22)}$$

It can be shown from the above, that the stresses and the other quantities are uniformly distributed throughout the rigid inclusion. The stress analysis alone predicts a composite yield stress that is independent of composition, the particle size and the degree of adhesion and/or interaction between the particle and the matrix.[9]

References

1. Rothon, R. Particulate-Filled Polymer Composites, Longman, ISBN:0-582-08782-1, 1995.
2. Ahmed, S.; Jones, F. R. Composites 1988, 19, 277.
3. Kovacevic, V.; Lucic, S.; Cerovecki, Z. Int J Adhesion Adhesives 1997, 17, 239.
4. Goodier, J. N. J Appl Mech 1933, 55, 39.
5. Harding, P. H.; Berg, J. C. J Adhes Sci Techol 1997, 11, 1063.
6. Nguyen, F. N.; Berg, J. Adhes Sci Technol 2004, 18, 1011.
7. Szyszkowski W.; King, J. Comput Struct 1995, 56, 345.
8. Beck, R. H.; Gratch, S.; Newman, S.; Rusch, K. C. Polym Lett 1968, 6, 707.
9. Wang, T. T.; Matsuo, M.; Kwei, T. K. J Appl Phys 1971, 42, 4188.
10. Spurr, O. K.; Niegisch, W. D. J Appl Polym Sci 1962, 6, 582.
11. Dekkers, M. E. J.; Heikens, D. J Mater Sci 1983, 18, 3281.
12. Ganesh V. V.; Chawla, N. Mater Sci Eng A 2005, 391, 342.
13. Thölén A. R; Yao, Y. J Colloid Interface Sci 2003, 268, 362.
14. Rutz, B. H.; Berg, J. C. J Adhesion Sci Tech 2011, 25, 2629.
15. Pukanszky, B.; Voros, G. Polym Compos 1996, 7, 384.